

A comparative study of model ingredients: fragmentation in heavy-ion collisions using quantum molecular dynamics model

SANJEEV KUMAR and SUNEEL KUMAR*

School of Physics and Material Science, Thapar University, Patiala-147004, Punjab (India)

*suneel.kumar@thapar.edu

Abstract. We aim to understand the role of NN cross-sections, equation of state as well as different model ingredients such as width of Gaussian, clusterisation range and different clusterisation algorithms in multifragmentation using quantum molecular dynamics model. We notice that all model ingredients have sizable effect on the fragment pattern.

Keywords. cross-section, model ingredients, quantum molecular dynamics, intermediate mass fragments, multifragmentation

PACS Nos 25.70.Pq, 25.70.-z, 24.10.Lx

1. Introduction

The study of heavy-ion collisions at intermediate energies ($50 \leq E \leq 1000 \text{ MeV/nucleon}$) provides a rich source of information for many rare phenomena such as multifragmentation, collective flow as well as particle production [1,2]. One can also shed light on the mechanism behind the fragmentation in highly excited nuclear systems. In this energy region, multifragmentation appears to be a dominant de-excitation channel apart from the other less populated channels of manifestation of liquid gas phase transition in finite nuclear systems [1,3,4]. In the literature, multifragmentation has also been considered as a gateway to nuclear equation of state [5,6]. Numerous investigations are cited in the literature which handle the de-excitation of nuclear system in multifragmentation [7–13].

The experimental analysis of the emission of intermediate mass fragments (IMF's), ($5 \leq A \leq A_{tot}/6$), has yielded several interesting observations: De Souza et al. [10] observed a linear increase in the multiplicity of IMF's with incident energies for central collisions. In this study, incident energy was varied between 35 and 110 MeV/nucleon. On the other hand, Tsang et al. [11] reported a rise and fall in the production of IMF's. The maximal value of the IMF's shifts from nearly central to peripheral collisions with the increase in the incident energy. More refined results were reported by Peaslee et al. [12] for the reaction of $^{84}_{36}\text{Kr} + ^{197}_{79}\text{Au}$ for incident energy between 35 and 400 MeV/nucleon. Their

analysis revealed that IMF's multiplicity first increases till 100 MeV/nucleon and then decreases slowly. These findings pose a stringent test for any theoretical model designed for the study of multifragmentation.

Theoretically, multifragmentation can be studied by statistical [2] as well as semi-classical [5] models, respectively. The relation between multifragmentation process and nuclear equation of state was extensively studied by several authors with in the statistical approach for intermediate energy heavy-ion collisions [2,4,6]. On the other hand, semi-classical dynamical models [5] are very useful for studying the reaction from the start to final state where matter is fragmented and cold. In addition, these models also give possibility to extract the information about the nuclear equation of state [13] and NN cross-section [1,5,14]. The interaction among nucleons (in a heavy-ion reaction) can be studied within the G-matrix, with its real part representing the mean field and complex part denotes the NN cross-section [1,5,14]. Note that the contribution of imaginary part of the interaction is nearly absent in the low energy process such as fusion, fission and radioactivity [15]. One often uses a parametrized form for the real and imaginary parts of the G-matrix. It is well accepted to use a density dependent Skyrme type interactions for the real part of the G-matrix. However, heavy-ion dynamics depends not only on the density but also on the entire momentum plane [7]. Therefore, it is advisable to use momentum dependent interactions additionally.

The exact nature of NN cross-section, on the other hand, is still an open question [7,14]. A large number of calculations exist in the literature suggesting different strength and forms of the NN cross-sections [14,16]. In a simple assumption of hard core radius of NN potential, one has often used a constant and isotropic cross-section of 40 mb. In other calculations, a constant and isotropic cross-section with magnitude between 20 and 55 mb is also used [14]. The most sensitive observable to pin down the NN cross-section is collective flow. Recent calculations advocated its strength between 35-40 mb [14]. We shall concentrate here on multifragmentation. Our present study will be based on the semi-classical model, namely, quantum molecular dynamics (QMD). In semi-classical model, one has to face the problem of the stability of nuclei. Several model ingredients such as width of the Gaussian (L), has been used as free parameter. It varies between 4.33 fm^2 to 8.66 fm^2 [5]. On the same time, one needs to identify the clusters with the help of clusterization algorithm. Different cluster recognition algorithms can also influence the fragmentation. Our present interest is to perform a comparative study of different model ingredients along with different NN cross-sections and to see whether it is possible to pin down the strength of NN cross-sections by QMD model or not.

Our article is organized as follow: we discuss the model briefly in section-II. Our results and discussions are given in section-III and we summarize the results in section-IV.

2. Quantum Molecular Dynamics (QMD) Model

The QMD model [1,5,7,14,17] is a time dependent N-body theory which simulates the time evolution of heavy-ion reactions on an event-by-event basis. It is based on the generalized variational principle. As with every variational approach, it requires the choice of a test wave function Φ . In the QMD approach, this is an N-body wave function with $6N$ time-

dependent parameters if nuclear system contains N nucleons.

The basic assumption of QMD model is that each nucleon is represented by coherent states of the form (we set $\hbar, c = 1$) which are characterized by 6 time dependent parameters, \vec{r}_i and \vec{p}_i , respectively.

$$\phi_i(\vec{r}, t) = \left(\frac{2}{L\pi} \right)^{3/4} \exp^{-(\vec{r}-\vec{r}_i)^2/L} \exp^{i(\vec{r}-\vec{r}_i) \cdot \vec{p}_i(t)}, \quad (1)$$

Here L is the width of the Gaussian distribution. This width varies between 4.33 and 8.66 fm^2 in the literature [5]. The total N -body wave function is assumed to be a direct product of the coherent states

$$\Phi = \prod_{i=1}^{A_T+A_P} \phi_i(\vec{r}, \vec{r}_i, \vec{p}_i, t) . \quad (2)$$

To calculate the time evolution of a system, we start out from the action

$$S = \int_{t_1}^{t_2} \mathcal{L}[\Phi, \Phi^*] dt \quad (3)$$

with the Lagrange functional

$$\mathcal{L} = \langle \Phi | i\hbar \frac{d}{dt} - H | \Phi \rangle . \quad (4)$$

The total time derivative includes the derivation with respect to parameters. The time evolution of parameters is obtained by the requirement that the action is stationary under the allowed variation of wave function. This leads to a Euler-Lagrange equation for each time-dependent parameter.

Thus, the variational principle reduces the time evolution of N -body Schrödinger equation to the time evolution equations of $6(A_T + A_P)$ parameters to which a physical meaning can be attributed. The equations of motion for the parameters \vec{p}_i and \vec{r}_i reads as:

$$\frac{d\vec{r}_i}{dt} = \frac{\partial \langle H \rangle}{\partial \vec{p}_i} ; \quad \frac{d\vec{p}_i}{dt} = - \frac{\partial \langle H \rangle}{\partial \vec{r}_i} \quad (5)$$

If $\langle H \rangle$ has no explicit time dependence, QMD conserves the energy and momentum by construction.

The nuclear dynamics of the QMD model can also be translated into a semi classical scheme. The Wigner distribution function f_i of a nucleon i^{th} can be easily derived from the test wave functions.

$$f_i(\vec{r}, \vec{p}, t) = \frac{1}{(\pi\hbar)^3} \exp^{-(\vec{r}-\vec{r}_i(t))^2 \cdot 2/L} \cdot \exp^{-(\vec{p}-\vec{p}_i(t))^2 \cdot L/2\hbar^2} \quad (6)$$

and the total Wigner density is the sum of those of all nucleons. Hence the expectation value of total Hamiltonian reads

$$\begin{aligned} \langle H \rangle &= \langle T \rangle + \langle V \rangle \\ &= \sum_i \frac{p_i^2}{2m_i} + \sum_i \sum_{j>i} \int f_i(\vec{r}, \vec{p}, t) V^{ij}(\vec{r}, \vec{r}) \\ &\quad \times f_j(\vec{r}, \vec{p}, t) d\vec{r} d\vec{r}' d\vec{p} d\vec{p}' \end{aligned} \quad (7)$$

Where V^{ij} is given as:

$$\begin{aligned}
 V^{ij}(\vec{r}, \vec{r}) &= V_{Skyrme}^{ij} + V_{Yukawa}^{ij} + V_{Coul}^{ij} + V_{mdi}^{ij} \\
 &= \left[t_1 \delta(\vec{r} - \vec{r}) + t_2 \delta(\vec{r} - \vec{r}) \rho^{\gamma-1} \left(\frac{\vec{r} + \vec{r}}{2} \right) \right] \\
 &\quad + t_3 \frac{\exp(-|\vec{r} - \vec{r}|/\mu)}{(|\vec{r} - \vec{r}|/\mu)} + \frac{Z_i Z_j e^2}{|\vec{r} - \vec{r}|} \\
 &\quad + t_4 \ln^2 [t_5 (\vec{p}_i - \vec{p})^2 + 1] \delta(\vec{r} - \vec{r})
 \end{aligned} \tag{8}$$

which consists of Skyrme, Yukawa, Coulomb and momentum dependent parts of the interaction and Z_i, Z_j are the charges of i^{th} and j^{th} baryons.

Further, potential part resulting from the convolution of the distribution function f_i and f_j with the Skyrme interactions V_{Skyrme} reads as :

$$V_{Skyrme} = \alpha \left(\frac{\rho_{int}}{\rho_0} \right) + \beta \left(\frac{\rho_{int}}{\rho_0} \right)^\gamma . \tag{9}$$

The two of the three parameters of equation of state are determined by demanding that at normal nuclear matter density, the binding energy should be equal to 16 MeV. The third parameter γ is usually treated as a free parameter. Its value is given in term of the compressibility:

$$\kappa = 9\rho^2 \frac{\partial^2}{\partial \rho^2} \left(\frac{E}{A} \right) . \tag{10}$$

The different values of compressibility give rise to Soft and Hard equations of state.

The momentum dependence (V_{mdi}) of NN interaction, which may optionally be used in the model, is fitted to experimental data [5] on the real part of the nucleon optical potential. This yields:

$$V_{mdi} = \delta \cdot \ln^2 (\varepsilon \cdot (\Delta \vec{p})^2 + 1) \cdot \left(\frac{\rho_{int}}{\rho_0} \right) . \tag{11}$$

The potential part of the equation of state resulting from the convolution of distribution functions f_i and f_j with Skyrme and momentum dependent interactions, reads as:

$$\begin{aligned}
 U &= \alpha \left(\frac{\rho_{int}}{\rho_0} \right) + \beta \left(\frac{\rho_{int}}{\rho_0} \right)^\gamma \\
 &\quad + \delta \cdot \ln^2 (\varepsilon \cdot (\Delta \vec{p})^2 + 1) \cdot \left(\frac{\rho_{int}}{\rho_0} \right) .
 \end{aligned} \tag{12}$$

For the value of constants and details, reader is referred to ref. [5]. The inclusion of MDI is labeled as Soft momentum dependent (SMD) and Hard momentum dependent (HMD) equations of state. In recent studies, momentum dependent forces are found to be essential part of dynamics.

During the propagation, two nucleon can collide if they satisfy the condition $|\vec{r}_i - \vec{r}_j| \leq$

$\sqrt{\sigma/\pi}$. In this procedure, a binary collision is blocked if the final state phase space is already occupied. The Pauli principle of the final state reduces the free cross-section to effective levels. Here we take different forms of NN cross-sections $[\sigma]$ to understand the influence on fragment production. We shall here use an energy dependent cross-section due to Cugnon and also different constant cross-sections ranging between 20 and 55 mb [5,7]. The nature and strength of cross-section σ is depicted as superscript to σ .

3. Results and discussion

We here simulate the symmetric reactions of $^{79}\text{Au}^{197} + ^{79}\text{Au}^{197}$ at incident energies of 100, 400, 600 and 1000 MeV/nucleon and over complete range of the impact parameter. The system size and asymmetry effects will be analyzed by further studying the reactions of $^{10}\text{Ne}^{20} + ^{13}\text{Al}^{27}$, $^{18}\text{Ar}^{40} + ^{21}\text{Sc}^{45}$, $^{36}\text{Kr}^{84} + ^{41}\text{Nb}^{93}$ and $^{54}\text{Xe}^{131} + ^{57}\text{La}^{139}$ at energies between 20 and 150 MeV/nucleon. The clusterisation at first instance is made using the minimum spanning tree (MST) method, in which, nucleons are bound if $R_{Clus} = |\vec{r}_1 - \vec{r}_2| \leq 4$ fm. [1,5].

In fig.1, we display the multiplicity of intermediate mass fragments (IMF's) as a function

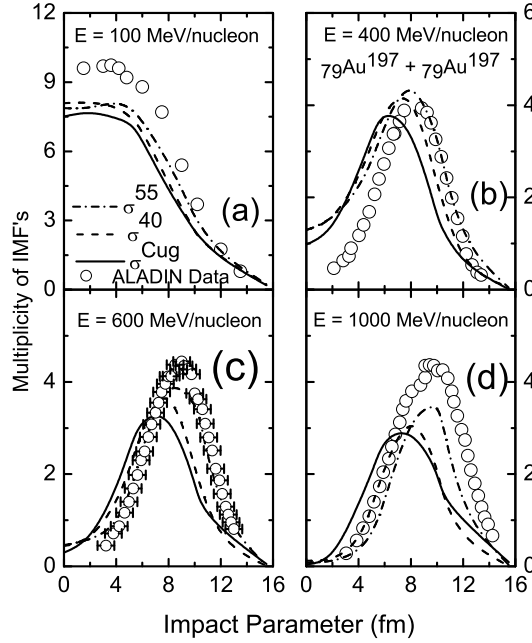


Figure 1. Comparison of average multiplicity of intermediate mass fragments (IMF's) with ALADIN data at incident energies of 100, 400 MeV/nucleon (top panel) and 600, 1000 MeV/nucleon (bottom panel) as a function of impact parameter. The results are displayed using soft momentum dependent (SMD) interactions.

of the impact parameter for the reaction of ${}_{79}\text{Au}^{197} + {}_{79}\text{Au}^{197}$ at incident energies 100, 400, 600 and 1000 MeV/nucleon. Here soft momentum dependent interaction (SMD) is used with different cross-sections. From the figure, the multiplicity of IMF's is maximal at 100 MeV/nucleon for smaller impact parameters, which decreases with the increase in the impact parameter. On the other hand, one sees a rise and fall in the multiplicity of the IMF's at higher incident energies. The dynamics at 100 MeV/nucleon, is mainly governed by the mean field or by the density of the reaction as compared to other higher incident beam energies under consideration (e.g. 400, 600 and 1000 MeV/nucleon). The incident energy of 30 MeV/nucleon is the lowest limit for any semi-classical model, where the effect of Pauli-blocking is $\approx 90\%$. Below this incident energy, quantum effects as well as pauli- blocking need to be redefined. There are no visible effects of different cross-sections at 100 MeV/nucleon. Due to the low excitation energy, central collisions generate better repulsion and break the colliding nuclei into IMF's, whereas for the peripheral collisions, the size of the fragment is close to the size of the reacting nuclei, therefore, one sees a very few IMF's. In contrary, a rise and fall can be seen at other higher incident energies. For the central collisions, the frequent NN collisions occurring at these energies do not allow any IMF's production, whereas, at peripheral collisions the energy transfer is from the participating matter to spectator matter is minimum, therefore, very few IMF's are seen. In all the cases, some effects of different NN cross-sections are visible at higher incident energies. The use of the momentum dependent interaction yields better comparison with ALADIN setup [18] for $\sigma = 55$ mb. This finding is in agreement with the results reported in ref. [1], where it was found that NN cross-section has sizable effect on reaction dynamics. Note that in these studies, static equation of state was used.

Let us now analyze the above effects in asymmetric reactions. In fig. 2, asymmetric reactions of ${}_{10}\text{Ne}^{20} + {}_{13}\text{Al}^{27}$, ${}_{18}\text{Ar}^{40} + {}_{21}\text{Sc}^{45}$, ${}_{36}\text{Kr}^{84} + {}_{41}\text{Nb}^{93}$ and ${}_{54}\text{Xe}^{131} + {}_{57}\text{La}^{139}$ are displayed as a function of beam energy at scaled impact parameter $b = 0.3$ (semi central collisions) using different cross-sections. Final results are also compared with the NSCL experimental data [19]. Due to no access to filters, no direct comparison with data could be made. These comparisons are just indicating the trend within theoretical framework. From the figure, it is clear that the trends of our calculations with soft momentum dependent (SMD) interactions are in good agreement with experimental data. Again different NN cross-sections fail to make any significant impact on the cluster dynamics.

One further see that the multiplicity of IMF's in ${}_{10}\text{Ne}^{20} + {}_{13}\text{Al}^{27}$ decreases with increase in the beam energies. For the reaction of ${}_{18}\text{Ar}^{40} + {}_{21}\text{Sc}^{45}$, similar trends emerge above 55 MeV/nucleon, as in case of ${}_{10}\text{Ne}^{20} + {}_{13}\text{Al}^{27}$. For energies below 55 MeV/nucleon, we see dominated role of mean field and hence increase in the intermediate mass fragments. For the rest of the reactions, namely, ${}_{36}\text{Kr}^{84} + {}_{41}\text{Nb}^{93}$ and ${}_{54}\text{Xe}^{131} + {}_{57}\text{La}^{139}$, the multiplicity of IMF's increases with the increase in the beam energy and cross-section. One should note that in the first two reactions, incident energy is much higher compared to the last two reactions.

Let us now understand how other technical parameters affect the fragmentation. In fig. 3, we display in the upper part, the effect of width of Gaussian wave packet. We display the results with narrow width ($L = 4.33 \text{ fm}^2$) and broad one ($L = 8.66 \text{ fm}^2$). We see that the variation of the width has sizable effect on clusterisation. A broader Gaussian results in extended interaction radius, therefore, binding more nucleons into a fragment. As a re-

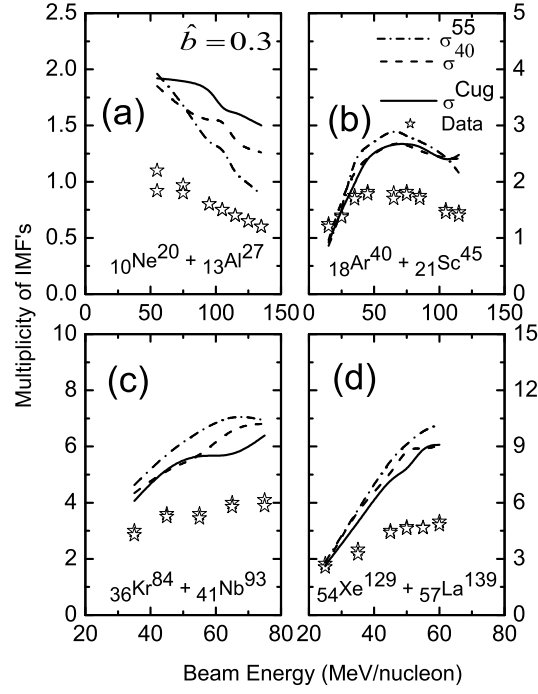


Figure 2. The average IMF's multiplicity versus beam energy in the reactions of $^{10}\text{Ne}^{20} + ^{13}\text{Al}^{27}$, $^{18}\text{Ar}^{40} + ^{21}\text{Sc}^{45}$, $^{36}\text{Kr}^{84} + ^{41}\text{Nb}^{93}$ and $^{54}\text{Xe}^{129} + ^{57}\text{La}^{139}$. The symbols represent the NSCL experimental results, while lines are representing the results obtained within QMD model using different cross sections σ^{55} , σ^{40} and σ^{Cug} .

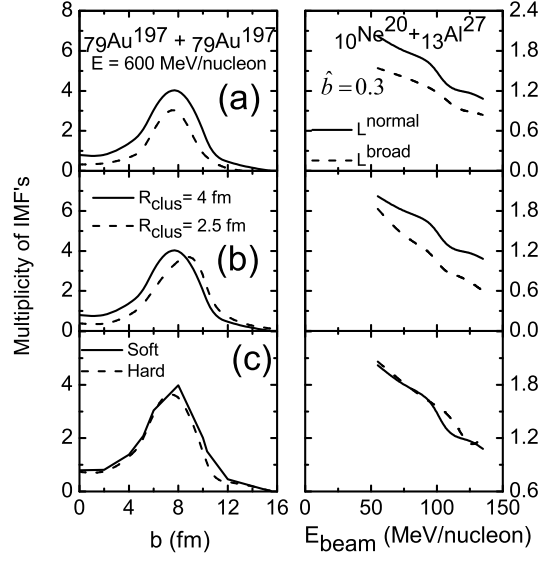


Figure 3. A Comparison of multiplicity of IMF's by employing different model ingredients like Gaussian width (upper panel), clusterisation cut off distance R_{clus} (middle) and equation of state (bottom). These results are displayed using soft (upper, middle, bottom) and hard (bottom) equation of state with σ^{55} .

sult, the fragment turns much heavier than the upper limit of IMF's (i.e 65 for (Au+Au) reaction) and hence there is net reduction in the production of IMF's. This result is in agreement with the findings in ref. [1]. One should also note that larger Gaussian width will also result in more attractive nuclear flow and hence will push the energy of vanishing flow towards higher incident energies. In the middle panel, we display the effect of cut off distance R_{clus} on clusterisation. We display the results with $R_{clus} = 4$ fm and a narrower one 2.5 fm. We see that when we choose a narrow cut off distance, lesser number of fragments are formed. In the bottom panel, we display the role of different equations of state by simulating the reactions with hard and soft equations of state. We see that different equations of state do not alter the results.

To further analyze the results, we display in fig. 4, the maximal number of intermediate mass fragments (N_{IMF}) as well as corresponding impact parameter as a function of the incident energy for the reaction of $^{197}_{79}\text{Au} + ^{197}_{79}\text{Au}$. Here apart from the different Gaussian widths and clusterisation distance, we also display the results with different clusterisation algorithms. Here we also use Simulated Annealing Clusterisation Algorithm (SACA) [1] to clusterise the phase space. In SACA approach [1], a group of nucleons can form a fragment if the total fragment energy/nucleon ζ is below a minimum binding energy:

$$\zeta = \sum_{i=1}^{N^f} \left[\sqrt{(\mathbf{p}_i - \mathbf{P}_{N^f}^{cm})^2 + m_i^2} - m_i + \frac{1}{2} \sum_{j \neq i}^{N^f} V^{ij}(\mathbf{r}_i, \mathbf{r}_j) \right] < L_{be} \times N^f, \quad (13)$$

with $L_{be} = -4.0$ MeV if $N^f \geq 3$ and $L_{be} = 0$ otherwise. In this equation, N^f is the number of nucleons in a fragment, $\mathbf{P}_{N^f}^{cm}$ is the center-of-mass momentum of the fragment. The requirement of a minimum binding energy excludes the loosely bound fragments which will decay after a while. To find the most bound configuration among the huge number of possible fragmentation patterns, we proceed as follow: we start from a random configuration which is chosen by dividing the whole system into few fragments. The energy of the individual clusters is calculated by summing over all nucleons present in that cluster using eqn.13. Note that as we neglect the interaction between fragments, the total energy calculated in this way differs from the total energy of the system. If the difference between the old and new energy is negative, the new configuration is accepted. If not, the new configuration may nevertheless be accepted with a probability of $\exp(-\Delta E/c)$, where c is the control parameter. This procedure is known as the Metropolis algorithm. The control parameter is decreased in small steps. This algorithm will yield eventually the most bound configuration. The identification of fragments using SACA is very time consuming. The algorithm searches the most bound configuration out of several million of different possibilities. The major outcome of this method is that we can recognize the fragments at relative high density.

From the figure, we see that different cross-sections yield quite similar trend. The absolute value varies with NN cross-sections as well as with other model ingredients. For example, we see that at 600 MeV/nucleon, the SACA method with 20 mb yields results close to the MST method with 55 mb. A broader Gaussian scales down the number and so is the case with reduced cut off distance. From this discussion, it is clear that the effect of larger cross-section (i.e. between 20 and 55 mb) is as large as effect of other model

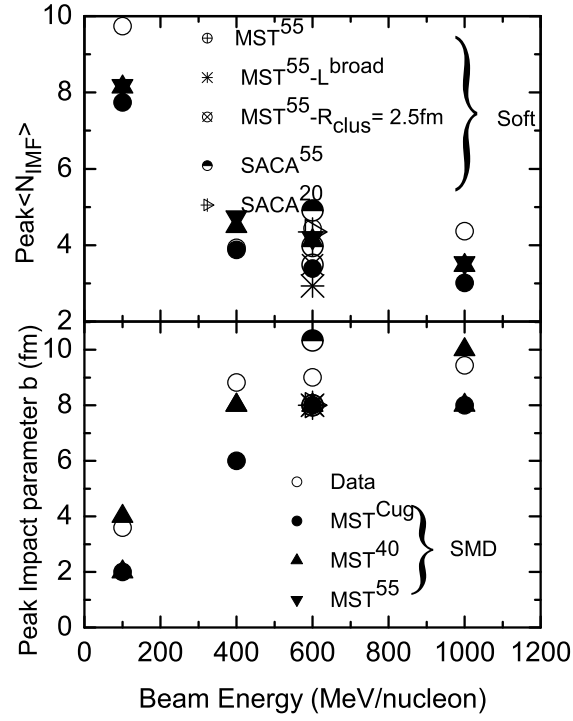


Figure 4. The Peak value of IMFs and corresponding impact parameter as a function of beam energy is compared with ALADIN data in the upper and bottom panels, respectively.

ingredients. Even a change of the clusterisation algorithm affect the outcome sizeably. From this analysis, one conclude that it may not be possible to pin down the magnitude of cross-section from multifragmentation since other technical parameters such as width of the Gaussian, clusterisation range or even the change of the clusterisation algorithm alters the results in similar fashion when semi-classical model such as quantum molecular dynamics is used.

4. Summary

In the present study, we focused on the comparative study of different model ingredients with semi-classical model, namely, quantum molecular dynamics (QMD) model. For this study, a hunt was made to compare our theoretical results of different cross-sections with experimental data. We also analyzed the results with model ingredients such as width of the Gaussian, clusterisation range and different clusterisation algorithms. We found that the effect of different cross-sections is of the order of the one obtained from the model ingredients. All model ingredients affect the fragmentation pattern in a similar fashion.

5. Acknowledgment

This work has been supported by the Grant no. 03(1062)06/ EMR-II, from the Council of Scientific and Industrial Research (CSIR) New Delhi, Govt. of India.

References

- [1] R. K. Puri, C. Hartnack, and J. Aichelin, Phys. Rev. C **54**, R28 (1996); P. B. Gassiaux *et al.*, Nucl. Phys. **A619**, 379 (1997); R. K. Puri and J. Aichelin, J. Comp. Phys. **162**, 245 (2000); Y. K. Vermani, S. Goyal, and R. K. Puri, J. Phys. G: Nucl. and Part. in press (2009); Y. K. Vermani and R. K. Puri, Eur. Phys. Lett. **85**, 62001 (2009).
- [2] J. P. Bondorf *et al.*, Phys. Rep. **257**, 133 (1995); J. P. Bondorf *et al.*, Nucl. Phys. **A443**, 321 (1985); Nucl. Phys. **A444**, 460 (1985); A. S. Botvina *et al.*, Nucl. Phys. **A584**, 737 (1995); A. S. Botvina and I. N. Mishustin, Eur. Phys. J. **A30**, 121 (2006); A. S. Botvina *et al.*, Phys. Lett. B **668**, 414 (2008); G. Casini *et al.*, Nucl-ex/0905.4703 (2005); S. Pal, S. K. Samaddar, and J. N. De, Nucl. Phys. **A608**, 49 (1996); D. K. Srivastava *et al.*, Nucl-th/0506075 (2005); L. Satpathy, M. Mishra, A. Das, M. Satpathy, Phys. Lett. B **237**, 181 (1990); C. B. Das, A. Das, L. Satpathy, M. Satpathy, Phys. Rev. C **53**, 1833 (1996).
- [3] J. B. Elliott *et al.*, Phys. Rev. C **49**, 3185 (1994); J. A. Hauger *et al.*, Phys. Rev. C **62**, 024616 (2000); P. F. Mastinu *et al.*, Phys. Rev. Lett. **76**, 2646 (1996); A. Bonasera *et al.*, Rivista del Nuovo Cimento **23**, 1 (2000); M. D'Agostino *et al.*, Phys. Lett. B **473**, 219 (2000).
- [4] I. N. Mishustin, Nucl. Phys. **A630**, 111 (1998); M. Mishra, M. Satpathy, and L. Satpathy, J. Phys. G: Nucl and Part. **14**, 1115 (1988).
- [5] C. Hartnack *et al.*, Eur. Phys. J. **A1**, 151 (1998); D. T. Khoa *et al.*, Nucl Phys. **A548**, 102 (1992); E. Lehmann, R. K. Puri, A. Faessler, G. Batko, and S. W. Huang, Phys. Rev. C **51**, 2113 (1995); R. K. Puri *et al.*, Nucl. Phys. **A575**, 733 (1994); C. Fuchs *et al.*, J. Phys. G: Nucl and Part. **22**,

- 131 (1996); E. Lehmann *et al.*, Prog. Part. Nucl. Phys. **30**, 219 (1993); E. Lehmann *et al.*, Z. Phys. **A355**, 55 (1996).
- [6] S. Pal, S. K. Samaddar, J. N. de, and B. Djerroud, Phys. Rev. C **57**, 3246 (1998); B. K. Srivastava *et al.*, (EOS collaboration) Phys. Rev. C **65**, 054617 (2002); A. Das, M. Mishra, M. Satpathy, and L. Satpathy, J. Phys. G: Nucl. and Part. **19**, 319 (1993).
- [7] J. Singh, S. Kumar, and R. K. Puri, Phys. Rev. C **62**, 044617 (2000); S. Kumar and R. K. Puri, *ibid.* **58**, 1618 (1998); Y. K. Vermani, S. Goyal, and R. K. Puri, *ibid.* **79**, 064613 (2009).
- [8] P. M. Milazzo *et al.*, Phys. Rev. C **66**, 021601(R) (2002).
- [9] C. A. Ogilvie *et al.*, Phys. Rev. Lett. **67**, 1214 (1991); N. T. B. Stone *et al.*, *ibid.* **78**, 2084 (1997); A. H. Raduta and A. R. Raduta Phys. Rev. C **65**, 054610 (2002).
- [10] R. T. de Souza *et al.*, Phys. Lett. B **268**, 6 (1991).
- [11] M. B. Tsang *et al.*, Phys. Rev. Lett. **71**, 1502 (1993); M. B. Tsang *et al.*, *ibid.* **102**, 122701 (2009).
- [12] G. F. Peaslee *et al.*, Phys. Rev. C **49**, R2271 (1994).
- [13] Q. Li, Z. Li, S. Soff, M. Bleicher, and H. Stöcker, J. Phys. G: Nucl. Part. Phys. **32**, 151 (2006).
- [14] A. D. Sood and R. K. Puri, Phys. Rev. C **70**, 034611 (2004); S. Kumar, M. K. Sharma, and R. K. Puri, *ibid.* **58**, 3494 (1998), A. D. Sood, R. K. Puri, and J. Aichelin, Phys. Lett. **B594**, 260 (2004); P. Danielewicz *et al.*, Science **298**, 1592 (2002).
- [15] R. K. Gupta, S. Singh, R. K. Puri, and W. Scheid, Phys. Rev. C **47**, 561 (1993); R. K. Gupta *et al.*, J. Phys. G: Nucl and Part. **18**, 1533 (1992); S. S. Malik, S. Singh, R. K. Puri, S. Kumar, and R. K. Gupta, Parmana J. Physics **32**, 419 (1989); R. K. Puri, S. S. Malik, and R. K. Gupta, Eur. Phys. Lett. **9**, 767 (1989); R. K. Puri and R. K. Gupta, J. Phys. G: Nucl. and Part. **18**, 903 (1992); R. K. Puri, M. K. Sharma, and R. K. Gupta, Eur. Phys. J. **A3**, 277 (1998); R. Arora, R. K. Puri and R. K. Gupta, Eur. Phys. J. **A8**, 103 (2000); R. K. Puri and R. K. Gupta, Phys. Rev. C **45**, 1837 (1992); R. K. Puri, P. Chattopadhyay, and R. K. Gupta, *ibid.* **43**, 315 (1991); R. K. Puri *et al.*, Eur. Phys. J. **A23**, 429 (2005).
- [16] G. Q. Li and R. Machleidt, Phys. Rev. C **48**, 1702 (1993); T. Alm, G. Ropke, W. Bauer, F. Daffin, and M. Schmidt, Nucl. Phys. **A587**, 815 (1995); Y. M. Zhang, C. M. Ko, B. A. Li, and B. Zhang, Phys. Rev. Lett. **83**, 2534 (1999); Q. Li, Z. Li, and G. Mao, Phys. Rev. C **62**, 014606 (2000); Q. Li, Z. Li, and E. Zhao, *ibid.* **69**, 017601 (2004); T. Gaitanos, C. Fuchs, and H. H. Wolter, Prog. Part. Nucl. Phys. **53**, 45 (2004); Y. Zhang, Z. Li, and P. Danielewicz, Phys. Rev. C **75**, 034615 (2007).
- [17] S. W. Huang *et al.*, Phys. Lett. **B298**, 41 (1993); G. Batko, A. Faessler, S. W. Huang, E. Lehmann, and R. K. Puri, J. Phys. G: Nucl. and Part. **20**, 461 (1994); S. W. Huang *et al.*, Prog. Part. Nucl. Phys. **30**, 105 (1993).
- [18] A. Schütteuf *et al.*, Nucl. Phys. **A607**, 457 (1996).
- [19] W. J. Llope *et al.*, Phys. Rev. C **51**, 1325 (1995).